J Incl Phenom Macrocycl Chem (2008) 62:353–361
DOI 10.1007/s10847-008-9478-5

ORIGINAL ARTICLE

Inclusion of aramid chains into the layered silicates through solution intercalation route

Sonia Zulfiqar · Muhammad Ilyas Sarwar

Received: 19 May 2008 / Accepted: 5 July 2008 / Published online: 19 July 2008

Abstract Aramid–organoclay nanocomposites were fabricated through solution intercalation technique. Montmorillonite was modified with *p*-amino benzoic acid in order to have compatibility with the matrix. The effect of clay dispersion and the interaction between clay and polyamide chains on the properties of nanocomposites were investigated using X-ray diffraction (XRD), transmission electron microscopy (TEM), tensile testing of thin films, differential scanning calorimetry (DSC), thermogravimetric analysis (TGA) and water uptake measurements. Excessive clay dispersion was achieved even on the addition of high proportions of clay. The structural investigations confirmed the formation of delaminated nanostructures at low clay contents and disordered intercalated morphology at higher clay loadings. The tensile behavior and thermal stability significantly amplified while permeability reduced with increasing dispersibility of organoclay in the polyamide matrix.

Keywords Intercalation · Composite materials · Polymers · Nanostructures · Mechanical testing

Introduction

Polymer–clay nanocomposites typically exhibited mechanical, thermal and gas barrier properties, which are superior to those of the corresponding pure polymers [1–15]. Unique properties of the nanocomposites are usually observed when the ultra fine silicate layers are homogenously dispersed throughout the polymer matrix at nanoscale. The uniform dispersion of silicate layers is usually desirable for maximum reinforcement of the materials. Due to the incompatibility of hydrophilic layered silicates and hydrophobic polymer matrix, the individual nanolayers are not easily separated and dispersed in many polymers. For this purpose, silicate layers are usually modified with an intercalating agent to obtain organically modified clay prior to use in nanocomposite formation. The selection of modifier is important because it can enlarge the clay galleries as well as improve the compatibility between clay and the polymer [1, 16]. The aliphatic polyamide/clay nanocomposites have thoroughly been studied [17–21] but aromatic polyamides have been paid no attention in this area. Aromatic polyamides are one of the most important classes of high performance polymers, because they posses excellent mechanical properties, thermal stability, chemical resistance and low flammability and are good substitute for ceramics and metals in the automotive, aerospace, and microelectronics industries. However, they encounter processing difficulties due to limited solubility in organic solvents and high glass transition or melting temperatures. It is a result of chain stiffness and intermolecular hydrogen bonding between amide groups [22–24]. Modification of these materials by increasing the solubility and lowering the glass transition temperatures while maintaining thermal stability are of particular interest. Copolycondensation is one of the possible ways for modification of aromatic polyamides. Among other approaches, addition of optimal minimum amount of meta linkages to produce a few kinks in the linear amide chains or incorporation of flexibilizing linkages [25, 26] into the main chain generally leads to a

S. Zulfiqar · M. I. Sarwar (✉)
Department of Chemistry, Quaid-i-Azam University, Islamabad 45320, Pakistan
e-mail: ilyassarwar@hotmail.com

M. I. Sarwar
Department of Materials Science and Engineering, University of Delaware, Newark 19716, USA

significant improvement in the solubility of aramid. Co-polyamides that contain aryl ether or aryl sulfone linkages generally have lower glass transition temperature, greater chain flexibility and tractability than their corresponding analogs without these groups in the backbone. Polymers containing both aryl ether and aryl sulfone linkages are amorphous, have low T_g and show good mechanical properties. The low T_g and also improved solubility are attributed to the flexible linkages that provide a polymer chain with a lower energy of internal rotation. Different hybrid materials based on soluble aramids and polyamides have already been reported [27–32].

Keeping in view the importance of aromatic polyamides, we attempted to synthesize aramid containing sulfone linkages in its backbone with enhanced solubility in organic solvents. Aramid was prepared by condensing 4-aminophenyl sulfone with isophthaloyl chloride in anhydrous dimethyl acetamide (DMAc). These aramid chains were endcapped with amine groups using 1% extra diamine and these chains were employed to synthesize nanocomposites with organoclay using solution intercalation method. Na-montmorillonite was intercalated with *p*-amino benzoic acid. The amine end of organifier was protonated for attachment to the negatively charged silicate layers while the free acid group of the swelling agent can react with the amine end-capped chains of the aramid diffused into the space between the silicate layers of the montmorillonite. Intercalating effect becomes strong and more permanent because a massive amount of aramid chains chemically connected to the swelling agent producing thermally stable and mechanically stronger nanocomposites. The organoclay so prepared was used to make nanocomposites with aramid matrix. The aim was to examine the morphology, mechanical, thermal and permeability of thin nanocomposite films obtained by solvent evaporation and to correlate these properties with the nanostructure.

Experimental

Materials

Isophthaloyl chloride (IPC) ≥98%, triethylamine (TEA) ≥99.5% and hydrochloric acid (>99%) was obtained from Fluka and used as such. 4-aminophenylsulfone (APS) 97%, montmorillonite K-10 (cation exchange capacity 119 meq/100 g), *p*-aminobenzoic acid (*p*-ABA) 99% and silver nitrate (99.9%) were obtained from Aldrich and used as received. *N,N*-dimethyl acetamide (DMAc) >99% was procured from Aldrich and dried over molecular sieves before use.

Intercalation of layered silicates

Organoclay was prepared by cationic exchange reaction between the pristine montmorillonite and organifier. In a 500 mL beaker, 0.048 mol of the organifier (*p*-ABA) was dissolved in 100 mL of deionized water at 80 °C and 4.8 mL of concentrated hydrochloric acid was dropped into the organifier solution. In another beaker, the pure montmorillonite (20 g) was preliminarily dispersed in deionized water at 80 °C using a mechanical stirrer. The organifier solution was poured into the suspension of the pristine montmorillonite and the mixture was vigorously agitated by a mechanical stirrer at 60 °C for 3 h. The cation exchanged clay particles were collected by filtration and washed with deionized water until no further formation of AgCl by an $AgNO_3$ test to confirm the absence of halide anions. The organoclay was dried in vacuum oven at 60 °C for 24 h and was crushed using a mortar and sieved by a copper griddle with 325-mesh. The organoclay in this study was coded as *p*-ABA-MMT and was used for the preparation of nanocomposites.

Synthesis of aromatic polyamide chains

Aromatic polyamide was synthesized by condensing 4-aminophenyl sulfone (0.05 mol) and isophthaloyl chloride (0.05 mol) using DMAc as solvent at low temperature (0 °C) under inert atmosphere. The reaction is highly exothermic and low temperature is essential to prevent any side reactions. Then the reaction mixture was allowed to come to room temperature after 1 h. Though the polymerization reaction is enormously rapid, however, stirring of the reaction mixture was continued for further 24 h to ensure completion of the reaction. In order to produce amine end-capped aramid chains, 1% of APS was added to the reaction mixture. The aramid was highly viscous and yellowish brown in colour. To remove HCl from the aramid solution, stochiometric amount of TEA was added with constant stirring for 3 h. Centrifugation was carried out in order to settle down the precipitates and pure aramid was decanted and served as stock solution for the nanocomposite synthesis. Scheme 1 shows the reactions involved in the formation of amine end-capped aramid chains.

Synthesis of nanocomposites

Aramid/clay nanocomposites were produced by solution intercalation method, in which different amounts of *p*-ABA-MMT (2 to 20-wt.%) were mixed with appropriate amounts of aramid solution to yield particular nanocomposite concentrations. To control the dispersibility of organoclay in polyamide matrix, constant stirring was

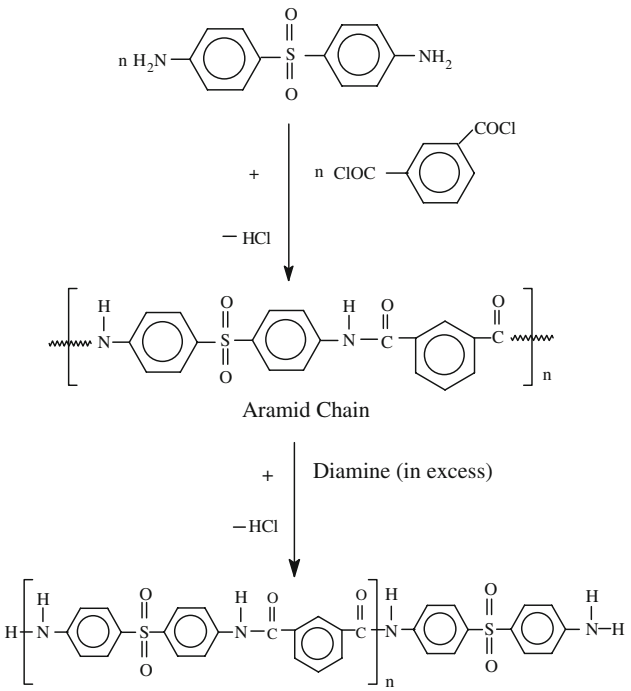

Scheme 1 Formation of amine end-capped aramid chains

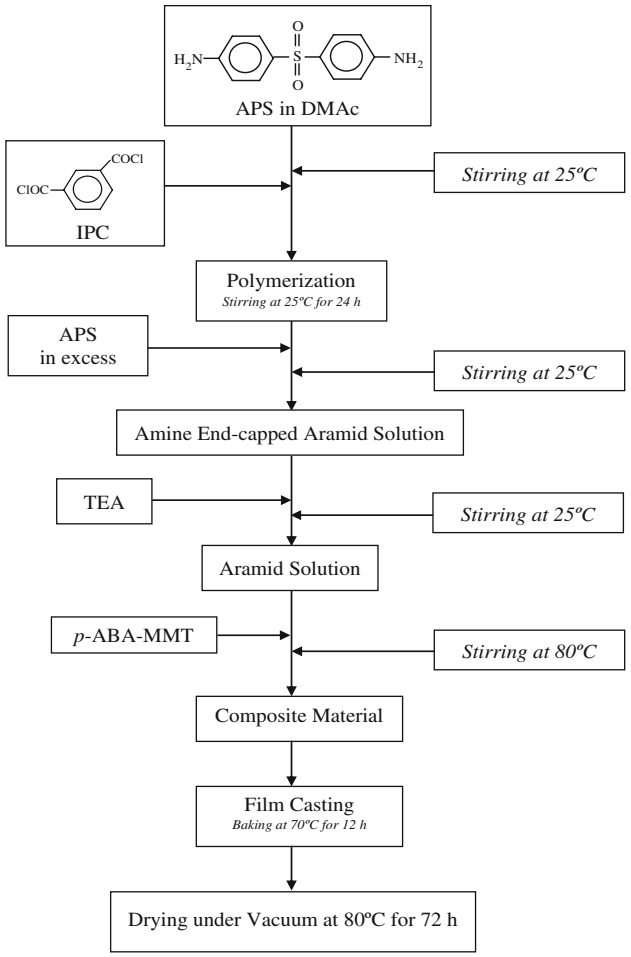

Scheme 2 Flow sheet diagram for the synthesis of aramid/*p*-ABA-MMT nanocomposites

applied at 80 °C for 1 h and then at 25 °C for 24 h. Nanocomposite films were cast by pouring the solutions for each concentration into petri dishes placed on a levelled surface followed by the evaporation of solvent at 70 °C for 12 h. Films were dried at 80 °C under vacuum to a constant weight. Schemes 2 and 3 show the flowsheet diagram and synthetic scheme for aramid/clay nanocomposites.

Characterization

Thin films of pristine aramid and nanocomposites were scanned in the reflection mode using a Philips PW 1820 diffractometer. Nickel-filtered Cu Kα radiation (radiation wavelength, $\lambda = 0.154$ nm) was produced by a PW 1729 X-ray generator at an operating voltage of 40 kV and a current of 30 mA. XRD measurements were carried out in the range 2–10° 2θ with a step size of 0.02° to measure the change in the interlayer spacing of clay. In order to investigate the internal morphology of the nanocomposites, thin films were first microtomed using Leica Ultracut UCT ultramicrotome into 60 nm ultra thin sections with a diamond knife and then examined under FEI Tecnai F20 transmission electron microscope operating at an accelerating voltage of 200 kV to record the images.

The tensile strength tests were carried out using Testometric Universal Testing Machine M350/500 according to DIN procedure 53455 and the crosshead speed was set at 5 mm min^{-1}. For each data point, five samples were tested, and the average value was taken. The thermogravimetric analyses of samples were carried out under nitrogen atmosphere with a METTLER TOLEDO TGA/SDTA 851^e thermogravimetric analyzer using 1–5 mg of the sample in Al_2O_3 crucible heated from 25 to 600 °C at a heating rate of 10 °C min^{-1} and a gas flow rate of 30 mL min^{-1}. Glass transition temperatures of samples were determined with a METTLER TOLEDO DSC 822^e differential scanning calorimeter using 5–10 mg of sample encapsulated in aluminium pans and heated at a ramp rate of 10 °C/min under nitrogen atmosphere.

The water absorption of aramid and nanocomposite films was carried out using a procedure under ASTM D570-81. The films were dried in a vacuum oven at 80 °C to a constant weight and then weighed to get the initial weight (W_o). The dried films were immersed in deionized water at 25 °C. After 24 h, the films were removed from water and then they were quickly placed between sheets of filter paper to remove the excess water and films were weighed immediately. The films were again soaked in

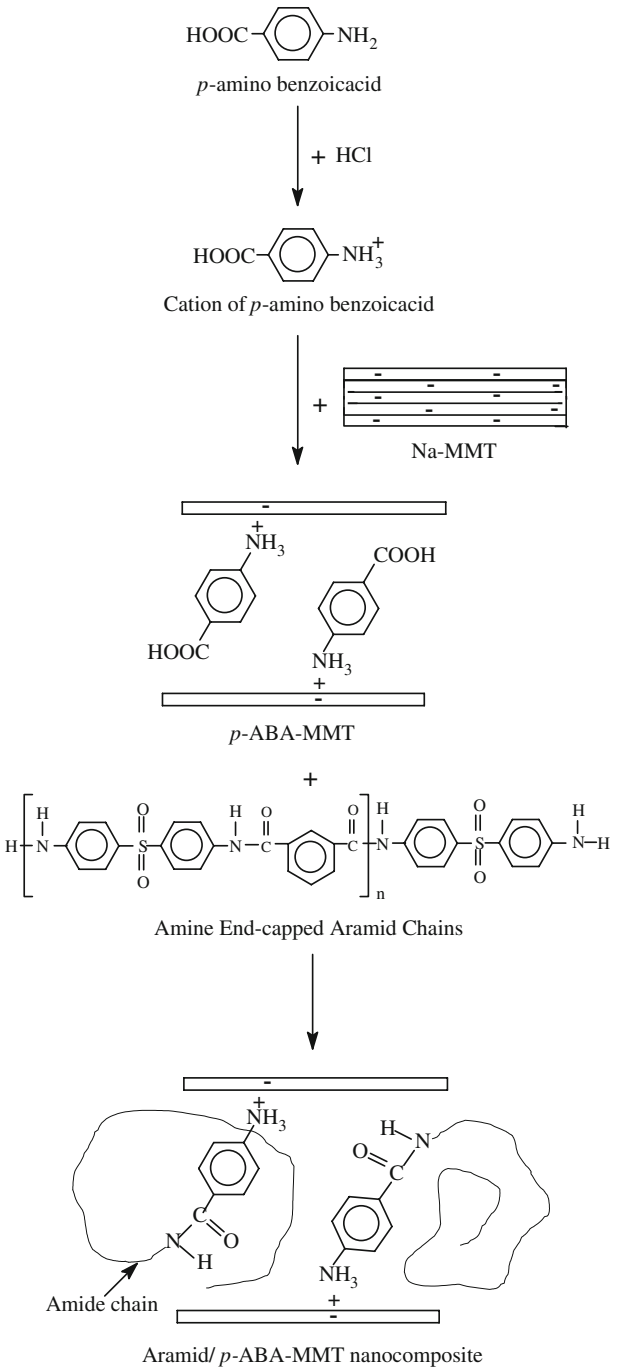

Scheme 3 Schematic representation for the formation of aramid nanocomposites with *p*-ABA-MMT

water. After another 24 h soaking period, the films were taken out, dried and weighed for any weight gain. This process was repeated again and again till the films almost attained the constant weight. The total soaking time was 168 h and the samples were weighed at regular 24 h time intervals to get the final weight (W_f). The percent increase in weight of the samples was calculated by using the formula $(W_f - W_o)/W_o$.

Results and discussion

Aramid film was transparent and yellowish brown in color. The incorporation of organoclay changed the color of films to dark yellowish brown. Moreover, a decrease in the transparency was observed at higher clay contents. The chemical structure, molecular weight and solution properties of aramid chains used in the formation of nanocomposites were illustrated in our recent reports [33, 34]. Aramid/*p*-ABA-MMT nanocomposites were characterized using various techniques as listed below.

X-ray diffraction

Figure 1 shows the XRD patterns of Na-MMT, *p*-ABA-MMT and the corresponding nanocomposites. The result reveals an increased *d*-spacing from 1.00 nm (8.78°) of Na-MMT to 1.49 nm (5.92°) of *p*-ABA-MMT indicating significant expansion of the clay galleries after cation exchange. The shift in the diffraction peak for *p*-ABA-MMT confirms that intercalation has been taken place and Na-MMT becomes organophilic in nature. Absence of diffraction peak in the range 2–10° 2θ for nanocomposites containing 2 to 20-wt.% of *p*-ABA-MMT is indicative of the disruption of ordered platelets leading to an exfoliated dispersion in aramid matrix. This is direct evidence that aramid/*p*-ABA-MMT nanocomposites have been formed as the nature of intercalating agent also affects the organoclay dispersion in the polymer matrix. In present study, the chemical interactions between acid group of swelling agent and amine end groups of the aramid chains led to more delaminated nanostructures. XRD result only reveals the relationship between the silicate layers, and it may be insufficient for the measurement of disordered or exfoliated nanostructures that fails to produce any peak in XRD pattern [35].

Transmission electron microscopy

In order to elucidate visually the extent of nanometer-scale clay dispersion in the aramid matrix, nanostructure of the composites were further analysed using TEM. The transmission electron micrographs of 6- and 10-wt.% clay nanocomposites are presented in Fig. 2a and b which shows a disruption of ordered platelets indicating dominating exfoliated dispersion. On the contrary, when the concentration of clay is increased to 20-wt.%, delaminated silicate layers existed along with ordered silicate conglomerations in the images but the dimensions of these conglomerations are too small to present a reflection peak in the XRD pattern rendering partially delaminated morphology of nanocomposites (Fig. 2c) with stacking of the nanolayers at higher clay loading. TEM micrographs of

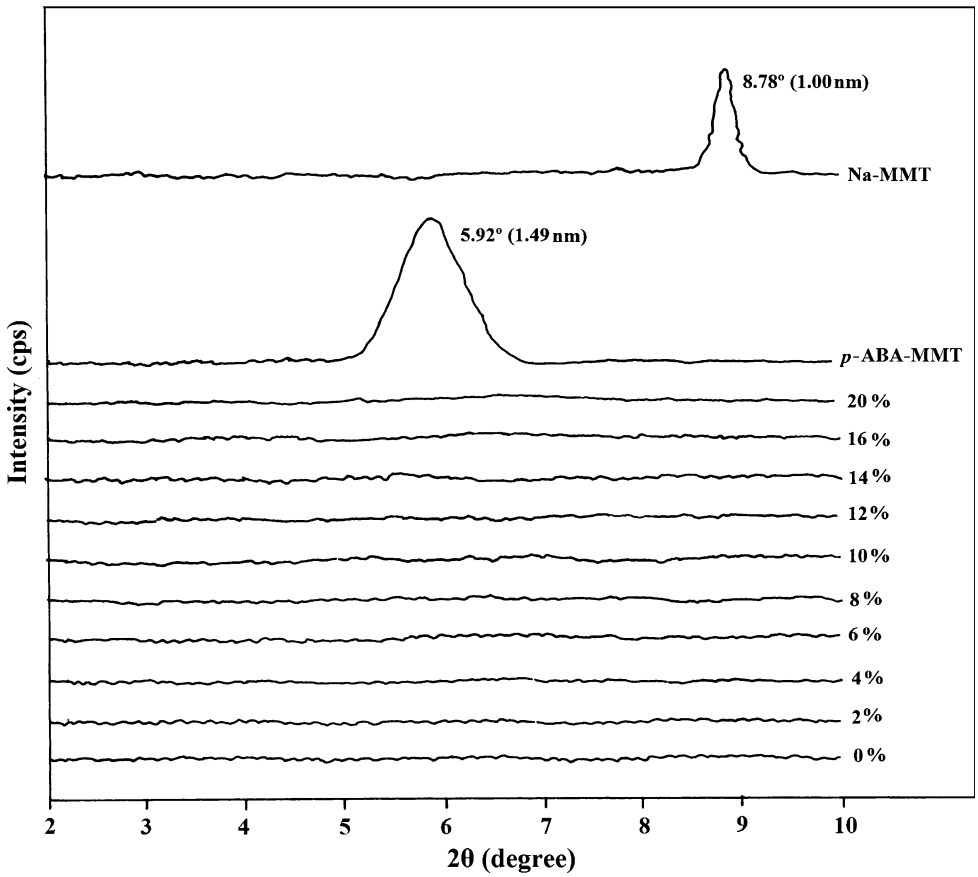

Fig. 1 X-ray diffraction patterns of aramid/*p*-ABA-MMT nanocomposites

these materials suggested delamination of organoclay in the aramid matrix up to 10-wt.% and presence of small stackings at higher concentrations.

Mechanical properties

The effect of organoclay content on the mechanical properties of aramid nanocomposites has been studied by tensile testing as reported in Table 1 and Fig. 3. The initial modulus of the aramid nanocomposites is higher compared to neat aramid, as result of delaminated structure. For instance, the modulus is significantly increased from 578.8 MPa for pure aramid to 1365.4 MPa for the composite that contains 6-wt.% of *p*-ABA-MMT. The stress at break, which is the ultimate strength that the material can sustain before breaking, increases up to 49.67 MPa with 6-wt.% *p*-ABA-MMT in the nanocomposites as compared with pure aramid (35.61 MPa). So, the stress and modulus increases up to 6-wt.% addition of organoclay in the composites and at higher concentrations it decreased. Addition of nanoclay also shows loss in the toughness and strain of the aramid clay nanocomposites. Thus the tensile measurements revealed that the effect of clay is more pronounced on the tensile modulus and strength. The marked increase in the tensile modulus reflects the reinforcement effect attained by the dispersion of clay nanolayer into aramid film. Also, the drop in the tensile properties was remarkable in the case of higher clay loading. This collapse of the mechanical properties can be attributed to the aggregation of clay nanolayers at higher concentrations.

Thermogravimetric analysis

Incorporation of organoclay also enhanced the thermal stability of the nanocomposites particularly up to 20-wt.%. Figure 4 shows the TGA traces of aramid/*p*-ABA-MMT nanocomposites under nitrogen atmosphere. Thus, we can speculate that interacting aramid chains between the clay layers serve to improve the thermal stability of nanocomposites. The addition of organoclay in optimum amount can significantly improve the thermal stability of aramid. The nanoscale dispersion of clay exhibits a barrier effect to the out diffusion of volatile decomposition products throughout the composite material. The thermal decomposition temperatures for the hybrids lie in the range of 225 °C to 450 °C. The residual weight loss in TGA is roughly proportional but does not match to the inorganic ratio introduced into the samples due to the loss of combined water from the clay at high temperature.

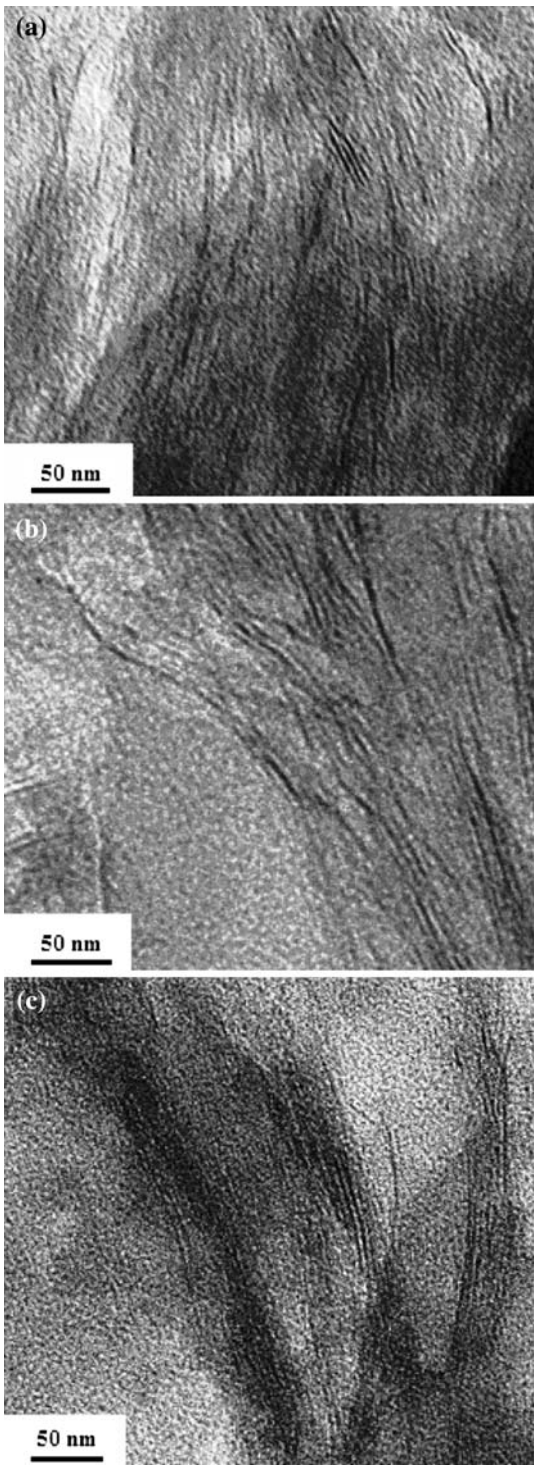

Fig. 2 TEM micrographs of aramid based nanocomposites containing (**a**) 6-wt.% (**b**) 10-wt.%, (**c**) 20-wt.% *p*-ABA-MMT

Differential scanning calorimetry

The thermal transitions and the effect of dispersed individual clay platelets on the glass transition temperatures of pure aramid and aramid/*p*-ABA-MMT nanocomposites were studied using DSC and data is presented in Fig. 5. All the nanocomposite materials (2 to 20 wt.%) are found to have a higher T_g value compared to the pristine aramid. The pure aramid exhibited the glass transition temperature at 78 °C which increased to 115 °C with the addition of clay up to 20-wt.%. This increased T_g resulted from the restricted segmental motions of the polymer chains at the organic–inorganic interface, due to the confinement of the aramid chains between the silicate layers, as well as the silicate surface–polymer interaction in the nanostructured hybrids. These results indicate that increase in T_g observed only when the silicate nanoplatelets were reasonably well delaminated and dispersed. It was also reported that majority of the other well dispersed polymer nanocomposites exhibited higher T_g than their corresponding pristine polymers [4, 36].

Water absorption measurements

The aromatic polyamide under investigation contains polar sulfonyl and amide groups in the backbone that have the tendency to uptake water through hydrogen bonding. Thus water absorption measurements become necessary for pure aramid and aramid/*p*-ABA-MMT nanocomposites and data is shown in Fig. 6. In the water permeability studies, we found that the incorporation of clay platelets into aramid matrix results in a decrease of water uptake relative to pure aramid by forming the tortuous path of water permeant. Water permeability depends on length, orientation and degree of delamination of layered silicate [37]. It should be noted that a further increase in clay concentration resulted in an enhanced barrier property of nanocomposites which may be attributed to the plate-like clays that effectively increase the length of the diffusion pathways, as well as decrease the water permeability.

Conclusions

The aramid/*p*-ABA-MMT nanocomposites were successfully prepared using solution intercalation method. The uniform dispersion of organoclay throughout the aramid matrix was confirmed by XRD and TEM analyses. The morphology, tensile properties, thermal stability and barrier property of aramid/clay nanocomposites were increased significantly with increasing the dispersibility of organoclay. Barrier property and thermal stability greatly increased with augmenting organoclay because the organoclay acts as the mass transport barrier to water molecules and volatile degraded products, respectively. The enhancements in the tensile strength and modulus of the nanocomposites by introducing organoclay may be due to the strong interactions between aramid matrix and

Table 1 Mechanical data of aramid/*p*-ABA-MMT composite materials

p-ABA-MMT contents (%)	Maximum stress (MPa) ±0.10	Maximum strain ±0.02	Initial modulus (MPa) ±0.02	Toughness (MPa) ±0.20
0.0	35.61	0.131	578.8	3.76
2.0	47.14	0.071	1073.2	2.38
4.0	48.49	0.065	1081.4	2.10
6.0	49.67	0.061	1365.4	2.09
8.0	47.79	0.059	1073.1	1.75
10.0	47.67	0.056	1042.6	1.70
12.0	47.21	0.054	1016.2	1.66
14.0	46.48	0.053	967.6	1.45
16.0	45.86	0.052	943.8	1.32
20.0	45.76	0.051	902.1	1.31

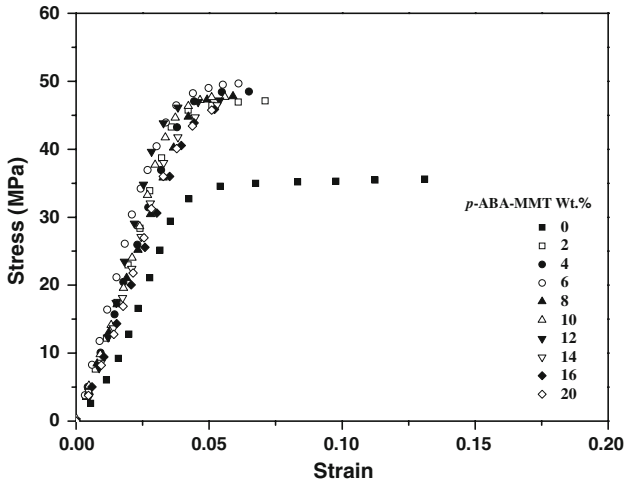

Fig. 3 Stress–strain curves of aramid/*p*-ABA-MMT nanocomposites

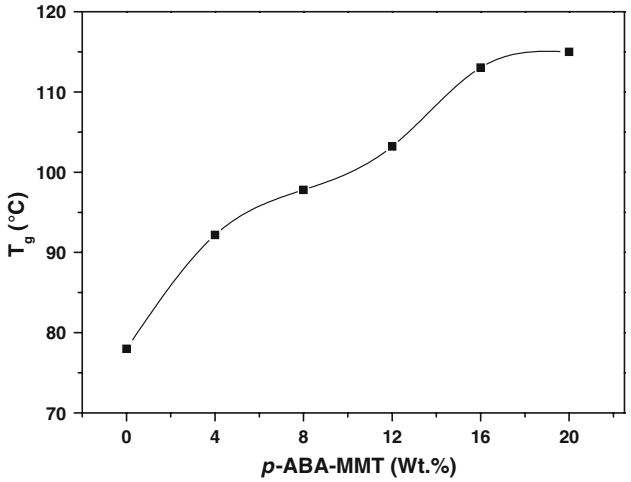

Fig. 5 Variation of glass transition temperatures as a function of *p*-ABA-MMT content in the nanocomposites

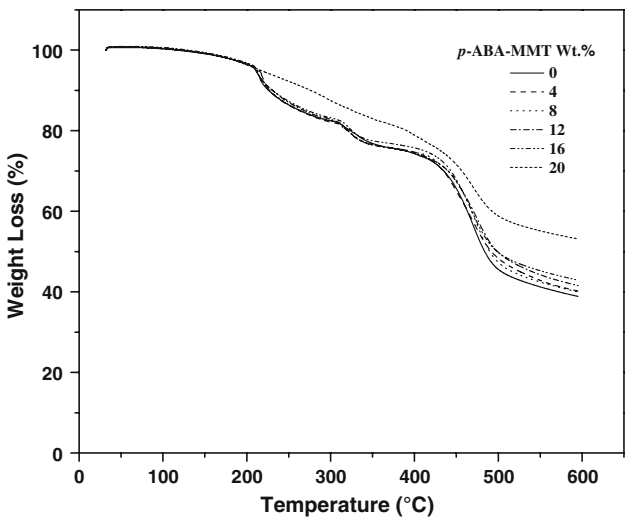

Fig. 4 TGA curves of aramid/*p*-ABA-MMT nanocomposites obtained at a heating rate of 10 °C min^{-1} in nitrogen

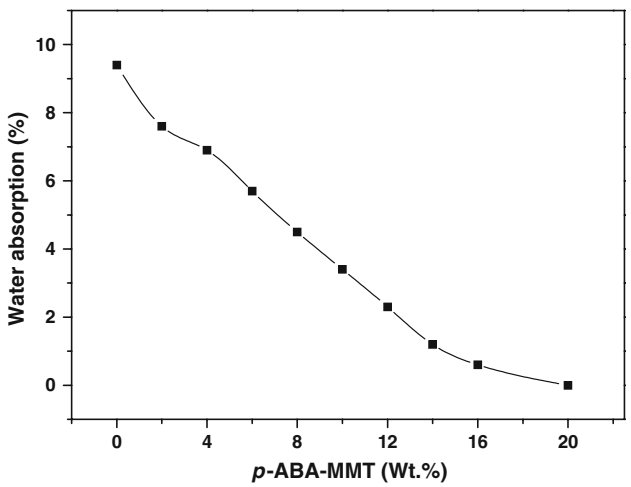

Fig. 6 Water absorption measurements of aramid/*p*-ABA-MMT nanocomposites at equilibrium

organoclay generating well exfoliation and dispersion of clay platelets in the aramid matrix.

Acknowledgements The authors appreciate the financial support provided by the Higher Education Commission of Pakistan (HEC) through project research grant 20-23-ACAD (R) 03-410. Sonia Zulfiqar is grateful to HEC for awarding her fellowship under "International Research Support Initiative Program" to pursue research work at Max Planck Institute for Polymer Research (MPI-P), Mainz, Germany. Special thanks are due to Prof. Dr. Gerhard Wegner, Director, MPI-P for providing the characterization facilities for the completion of this work.

References

1. Giannelis, E.P.: Polymer layered silicate nanocomposites. Adv. Mater. **8**, 29–35 (1996). doi:10.1002/adma.19960080104
2. Komarneni, S.: Feature article. Nanocomposites. J. Mater. Chem. **2**, 1219–1230 (1992). doi:10.1039/jm9920201219
3. Yano, Y., Usuki, A., Kurauchi, T., Kamigato, O.: Synthesis and properties of polyimide-clay hybrid. J. Polym. Sci. Part Polym. Chem. **31**, 2493–2498 (1993). doi:10.1002/pola.1993.080311009
4. Zulfiqar, S., Ahmad, Z., Ishaq, M., Saeed, S., Sarwar, M.I.: Thermal and mechanical properties of SEBS-g-MA based inorganic composite materials. J. Mater. Sci. **42**, 93–100 (2007). doi:10.1007/s10853-006-1082-8
5. Vaia, R.A., Vasudevan, S., Krawiec, W., Scanlon, L.G., Giannelis, E.P.: New polymer electrolyte nanocomposites: melt intercalation of poly (ethylene oxide) in mica-type silicates. Adv. Mater. **7**, 154–156 (1995). doi:10.1002/adma.19950070210
6. Sikka, M., Cerini, L.N., Ghosh, S.S., Winey, K.I.: Melt intercalation of polystyrene in layered silicates. J. Polym. Sci. Part B Polym. Phys. **34**, 1443–1449 (1996). doi:10.1002/(SICI)1099-0488(199606)34:8<1443::AID-POLB7>3.0.CO;2-T
7. Zilg, C., Mulhaupt, R., Finter, J.: Morphology and toughness/stiffness balance of nanocomposites based upon anhydride-cured epoxy resins and layered silicates. Macromol. Chem. Phys. **200**, 661–670 (1999). 10.1002/(SICI)1521-3935(19990301)200:3<661::AID-MACP661>3.0.CO;2-4
8. Messersmith, P.B., Giannelis, E.P.: Synthesis and characterization of layered silicate-epoxy nanocomposites. Chem. Mater. **6**, 1719–1725 (1994). doi:10.1021/cm00046a026
9. Xu, R., Manias, E., Snyder, A.J., Runt, J.: New biomedical poly(urethane urea)-layered silicate nanocomposites. Macromolecules **34**, 337–339 (2001). doi:10.1021/ma0013657
10. Burnside, S.D., Giannelis, E.P.: Synthesis and properties of new poly (dimethyl siloxane) nanocomposites. Chem. Mater. **7**, 1597–1600 (1995). doi:10.1021/cm00057a001
11. Kausar, A., Zulfiqar, S., Shabbir, S., Ishaq, M., Sarwar, M.I.: Mechanical properties of functionalized SEBS based inorganic hybrid materials. Polym. Bull. **59**, 457–468 (2007). doi:10.1007/s00289-007-0786-5
12. Bibi, N., Sarwar, M.I., Ishaq, M., Ahmad, Z.: Mechanical and thermal properties of nanocomposites of poly(vinyl chloride) and co-poly(vinyl chloride-vinyl alcohol-vinyl acetate) with montmorillonite. Polym. Polym. Compos. **15**, 313–319 (2007)
13. Zulfiqar, S., Sarwar, M.I.: Mechanical and thermal behavior of clay reinforced aramid nanocomposite materials. Scr. Mater. **59**, 436–439 (2008). doi:10.1016/j.scriptamat.2008.04.021
14. Fornes, T.D., Yoon, P.J., Keskkula, H., Paul, D.R.: Nylon 6 nanocomposites: the effect of matrix molecular weight. Polymer (Guildf.) **42**, 09929–09940 (2001). doi:10.1016/S0032-3861(01)00552-3
15. Fornes, T.D., Yoon, P.J., Hunter, D.L., Keskkula, H., Paul, D.R.: Effect of organoclay structure on nylon 6 nanocomposite morphology and properties. Polymer (Guildf.) **43**, 5915–5933 (2002). doi:10.1016/S0032-3861(02)00400-7
16. Chen, G.M., Ma, Y.M., Qi, Z.N.: Preparation of polystyrene/toluene-2,4-di-isocyanate-modified montmorillonite hybrid. J. Appl. Polym. Sci. **77**, 2201–2205 (2000). doi:10.1002/1097-4628(20000906)77:10<2201::AID-APP13>3.0.CO;2-L
17. Okada, A., Kawasumi, M., Usuki, A., Kojimi, Y., Kurauchi, T., Kamigato, O.: Synthesis and properties of nylon-6/clay hybrids. Mater. Res. Symp. Proc. **171**, 45–50 (1990)
18. Usuki, A., Kojima, Y., Kawasumi, M., Okada, A., Fukushima, Y., Kurauchi, T., Kamigaito, O.: Synthesis of nylon 6-clay hybrid. J. Mater. Res. **8**, 1179–1184 (1993). doi:10.1557/JMR.1993.1179
19. Hoffmann, B., Kressler, J., Stopplemann, G., Friedrich, C., Kim, G.-M.: Rheology of nanocomposites based on layered silicates and polyamide-12. Colloid Polym. Sci. **278**, 629–636 (2000). doi:10.1007/s003960000294
20. Liu, X., Wu, Q., Zhang, Q., Berglund, L.A., Mo, Z.: High-temperature X-ray diffraction studies on polyamide6/clay nanocomposites upon annealing. Polym. Bull. **48**, 381–387 (2002). doi:10.1007/s00289-002-0051-x
21. Ayyer, R.K., Leonov, A.I.: Comparative rheological studies of polyamide-6 and its low loaded nanocomposite based on layered silicates. Rheol. Acta. **43**, 283–292 (2004)
22. Cassidy, P.E.: Thermally Stable Polymers. Dekker, New York (1980)
23. Frazer, A.H.: High Temperature Resistant Polymers. Wiley, New York (1968)
24. Yang, H.H.: Aromatic High-Strength Fibers, pp. 66–289. Wiley, New York (1989)
25. Zulfiqar, S., Ahmad, Z., Sarwar, M.I.: Soluble aromatic polyamide bearing ether linkages: synthesis and characterization. Colloid Polym. Sci. **285**, 1749–1754 (2007). doi:10.1007/s00396-007-1768-8
26. Zulfiqar, S., Lieberwirth, I., Sarwar, M.I.: Soluble aramid containing ether linkages: synthesis, static and dynamic light scattering studies. Chem. Phys. **344**, 202–208 (2008). doi:10.1016/j.chemphys.2008.01.002
27. Sarwar, M.I., Zulfiqar, S., Ahmad, Z.: Poly (ether amide) and silica nanocomposites derived from sol–gel process. J. Sol-Gel Sci. Technol. **45**, 89–95 (2008). doi:10.1007/s10971-007-1640-9
28. Sarwar, M.I., Zulfiqar, S., Ahmad, Z.: Organic-inorganic nanocomposites prepared from fluoro-aramid and silica. Colloid Polym. Sci. **285**, 1733–1739 (2007). doi:10.1007/s00396-007-1760-3
29. Sarwar, M.I., Zulfiqar, S., Ahmad, Z.: Polyamide-silica nanocomposites: mechanical, morphological and thermomechanical investigations. Polym. Int. **57**, 292–296 (2008). doi:10.1002/pi.2343
30. Sarwar, M.I., Zulfiqar, S., Ahmad, Z.: Preparation and properties of polyamide-titania nanocomposites. J. Sol-Gel Sci. Technol. **44**, 41–46 (2007). doi:10.1007/s10971-007-1591-1
31. Sarwar, M.I., Zulfiqar, S., Ahmad, Z.: Properties of polyamide-zirconia nanocomposites prepared from sol-gel technique. Polym. Compos. (2008). doi:10.1002/pc.20538
32. Ahmad, Z., Sarwar, M.I., Mark, J.E.: Thermal and mechanical properties of aramid-based titania hybrid composites. J. Appl. Polym. Sci. **70**, 297–302 (1998). doi:10.1002/(SICI)1097-4628(19981010)70:2<297::AID-APP9>3.0.CO;2-P
33. Zulfiqar, S., Sarwar, M.I.: Soluble aromatic polyamide bearing sulfone linkages: synthesis and characterization. High. Perform Polym. (2008). doi:10.1177/0954008308089114
34. Zulfiqar, S., Ishaq, M., Ahmad, Z., Sarwar, M.I.: Synthesis, static, and dynamic light scattering studies of soluble aromatic polyamide. Polym. Adv. Technol. (2008). doi:10.1002/pat.1120
35. Morgan, A.B., Gilman, J.W.: Characterization of polymer-layered silicate (clay) nanocomposites by transmission electron microscopy and X-ray diffraction: a comparative study. J. Appl. Polym. Sci. **87**, 1329–1338 (2003). doi:10.1002/app.11884

36. Li, Y., Zhao, B., Xie, S., Zhang, S.: Synthesis and properties of poly(methyl methacrylate)/montmorillonite (PMMA/MMT) nanocomposites. Polym. Int. **52**, 892–898 (2003). doi:10.1002/pi.1121

37. Bharadwaj, R.K.: Modeling the barrier properties of polymer-layered silicate nanocomposites. Macromolecules **34**, 9189–9192 (2001). doi:10.1021/ma010780b